Molecular Dynamics Study of a Lithium Ion in Ammonia

S. V. Hannongbua*, T. Ishida**, E. Spohr, and K. Heinzinger
Max-Planck-Institut für Chemie (Otto-Hahn-Institut), Mainz, Federal Republic of Germany

Z. Naturforsch. **43a**, 572–582 (1988); received March 18, 1988

A Molecular Dynamics simulation of a solution of one Li^+ in 215 NH_3 molecules has been performed at an average temperature of 235 K. A newly developed flexible model for NH_3 is employed and the Li^+-NH_3 interactions are derived from ab initio calculations. The structure of the solution is described by radial distribution functions and the orientation of the molecules. A solvation number of six is found for Li^+ and a strong preference of the solvation shell molecules exists for an orientation where the Li^+-N vector and the dipole moment direction of NH_3 are parallel. The self-diffusion coefficient, the hindered translational motions and librations are calculated separately for the ammonia molecules in the solvation shell and in the bulk. The effect of Li^+ on intramolecular geometry and vibrations is reported.

I. Introduction

The physics of metal solutions in liquid ammonia is an interesting topic in modern physical chemistry. For example, striking differences between solvation of metal atoms in water and liquid ammonia exist. Dissolving alkali metal atoms in water leads to oxidation to the monovalent cations, the formation of hydroxide ions, and H_2 evolution. On the contrary, in liquid ammonia free electrons exist if the alkali metal concentration exceeds a few mole percent [1]. The electrical conductivity of a 20 mole percent lithium solution is higher than that of liquid mercury at room temperature [2].

Structural information about bulk ammonia as well as metal ion and electron solvation is necessary in order to understand the properties of these solutions. The only X-ray scattering experiment on liquid ammonia reported so far has been performed by Narten [3]. Only the nitrogen-nitrogen radial distribution function (RDF) can be extracted reliably from these data. The available neutron scattering data [4] are not analysed in terms of atom-atom RDFs. Neutron scattering experiments with isotopic substitution, which yield information also about the nitrogen-hydrogen and hydrogen-hydrogen RDFs, have not been performed.

Considerable efforts have been made in attempts to overcome this lack of experimental information on liquid ammonia by means of computer simulations [5–9], which yield information about all three atom-atom RDFs. Recently, the electron solvation in liquid ammonia has been treated by the quantum path integral Monte Carlo method on the basis of a pseudopotential ansatz for the electron ammonia interactions [10].

In this work, the structure of the solvation shell of a lithium ion dissolved in NH_3 will be discussed in detail and compared with some preliminary results from a neutron diffraction experiment [4] and a recent Molecular Dynamics (MD) simulation [11]. In addition, the dynamical properties of ammonia in the bulk and in the solvation shell of the ion have been calculated separately from the simulation and are compared with experimental data. The flexibility of the ammonia model employed permits the investigation of the effect of Li^+ on the intramolecular vibrations of NH_3 and the comparison of the calculated gas-liquid frequency shifts with IR and Raman measurements.

II. Potential Functions

A flexible four-site model was employed to describe the ammonia-ammonia interactions. The experimental gas phase geometry, with an N-H distance of 1.0124 Å and an HNH angle of 106.67°, was taken from [12]. The partial charges of $0.2674|e|$ on the hydrogen and $-0.8022|e|$ on the nitrogen atom are taken from SCF calculations of the ammonia molecule [5]. The Coulomb interaction is supplemented by

* Permanent address: Department of Chemistry, Faculty of Science, Chulalongkorn University, Bangkok 10500, Thailand.
** Permanent address: Department of Chemistry, State University of New York at Stony Brook, Stony Brook, N.Y. 11794, USA.

Reprint requests to Dr. K. Heinzinger, Max-Planck-Institut für Chemie, Saarstraße 23, D-6500 Mainz.

0932-0784 / 88 / 0600-0572 $ 01.30/0. – Please order a reprint rather than making your own copy.

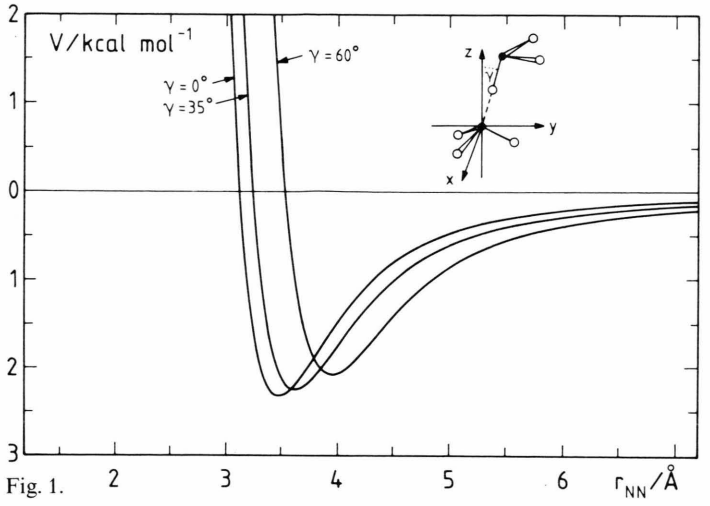

Fig. 1. Ammonia-ammonia pair potentials as a function of nitrogen-nitrogen distance for three orientations as shown in the insertion.

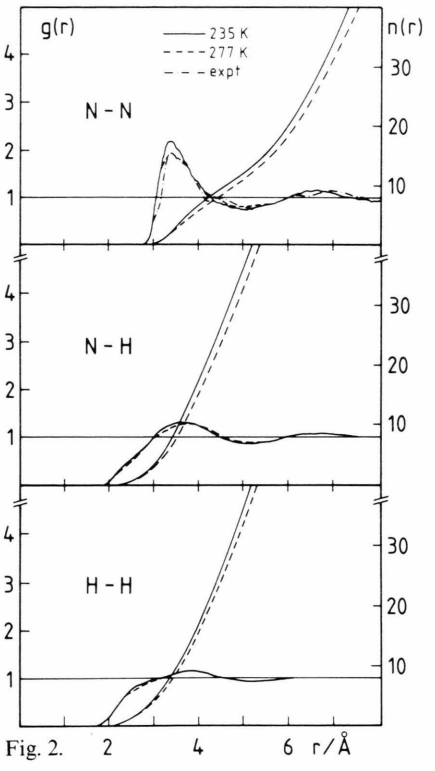

Fig. 2. Nitrogen-nitrogen, nitrogen-hydrogen and hydrogen-hydrogen radial distribution functions and running integration numbers for a Li^+-ammonia solution at 235 K and 277 K. The experimental nitrogen-nitrogen radial distribution function at 277 K is also given for comparison.

a (12-6) Lennard-Jones potential, a Morse potential, and a Born-Mayer potential function in the interactions between two nitrogen atoms, a nitrogen and a hydrogen atom, and two hydrogen atoms, respectively. The parameters were adjusted to give satisfactory agreement for the structure and binding energy of the dimer. The potential functions are summarized in Table 1.

Figure 1 shows the variation of the ammonia-ammonia interaction potential as a function of the nitrogen-nitrogen distance for three orientations as indicated in the insertion. The depth of the potential changes only slightly in the given range of orientations. Therefore, in agreement with simulation results discussed below, there is no strong preference for a hydrogen bond along the lone pair direction. However, the distance where the minimum occurs changes considerably.

Several intramolecular potential surfaces for the ammonia molecule are given in the literature [13–15]. They are all based on spectroscopic data. In this study we decided to use the surface by Spirko [14], which accounts for the inversion mode of the molecule by means of a strongly anharmonic potential. The potential function is given by

$$V_{\text{intra}} = \sum_{u=1}^{4} k_u h^{2u} + k'_1 h^2 s_1 + k'_2 h^4 s_1 + \frac{1}{2} \sum_{1=i\neq j}^{5} F_{ij} s_i s_j + \sum_{1=i\leq j\leq k}^{5} F_{ijk} s_i s_j s_k + \sum_{1=i\leq j\leq k\leq l}^{5} F_{ijkl} s_i s_j s_k s_l . \quad (1)$$

The symmetry coordinates s_i are defined as

$$s_1 = \frac{1}{\sqrt{3}}(\Delta r_1 + \Delta r_2 + \Delta r_3),$$

$$s_2 = \frac{1}{\sqrt{6}}(2\Delta r_1 - \Delta r_2 - \Delta r_3),$$

$$s_3 = \frac{1}{\sqrt{6}}(2\Delta\alpha_1 - \Delta\alpha_2 - \Delta\alpha_3), \quad (2)$$

$$s_4 = \frac{1}{\sqrt{2}}(\Delta r_2 - \Delta r_3), \quad s_5 = \frac{1}{\sqrt{2}}(\Delta\alpha_2 - \Delta\alpha_3),$$

where Δr_i and $\Delta\alpha_i$ are the three N–H distances and H–N–H angles, respectively. h is the distance of the

nitrogen atom from the plane spanned by the three hydrogen atoms. The non-vanishing force constants have been calculated from the data in [14] and are summarized in Appendix A.

The Li^+-N and Li^+-H potentials were obtained from ab initio calculations with a Double Zeta basis set which included polarization functions. The C_{3v}-symmetry is the energetically most favourable configuration. The Li^+-N distance at the minimum position is 2.0 Å and the stabilization energy is -167 kJ/mol. Further details of the ab initio calculations and the fitting procedure, in which also the Coulomb contribution was allowed to vary, are given in [16]. The final parameters are included in Table 1.

III. Details of the Simulation

In order to be able to neglect the influence of free electrons on the Li^+-ammonia interactions the simulation was performed for a dilute solution consisting of one Li^+ and 215 ammonia molecules. With the experimental density of 0.690 g/cm^3 at 235 K and atmospheric pressure the resulting box length of the basic cube was 20.66 Å. The shifted force method [17] has been used with a cut-off length of half the box size. Periodic boundary conditions were employed.

The starting configuration was derived from a simulation of bulk ammonia by substituting one NH_3 molecule by one Li^+ and subsequent equilibration. The simulation was performed at an average temperature of 235 K and extended over 3.75 picoseconds (15 000 time steps of $2.5 \cdot 10^{-16}$ s length). An additional simulation of the system at 277 K and a density of 0.633 g/cm^3, corresponding to about 5 bar, was performed and lasted for 3 picoseconds.

Table 1. Intermolecular potentials employed in the simulation. Energies are given in units of 10^{-19} J with the distances in Å.

$$V_{NN}(R) = 14.85/R + 55719/R^{12} - 13.6/R^6$$
$$V_{NH}(R) = -4.95/R + 0.01042\{\exp[-4.6(R-2.4)] - 2\exp[-2.3(R-2.4)]\}$$
$$V_{HH}(R) = 1.65/R + 48.64\exp(-3.7R)$$
$$V_{LiN}(R) = -52.91/R + 3043/R^6 + 745\exp(-5.3R)$$
$$V_{LiH}(R) = 17.62/R + 2167/R^6 + 3.81\exp(-0.58R)$$

IV. Results and Discussion

a) Solvent Structure

Due to the fact that there is only one ion per 215 ammonia molecules, the solvent properties discussed in this chapter are within the limits of statistical error identical with those of pure liquid ammonia.

The atom-atom RDFs, $g_{\alpha\beta}(r)$, for the ammonia molecules are shown in Fig. 2 for two different temperatures together with the running coordination numbers $n_{\alpha\beta}(r)$ defined as

$$n_{\alpha\beta}(r) = 4\pi\varrho_\beta \int_0^r g_{\alpha\beta}(r')\, r'^2\, dr', \tag{3}$$

where ϱ_β is the number density of species β. Characteristic values of the RDFs at 235 and 277 K are given in Table 2.

The N–N RDF from the X-ray measurements by Narten [3] at 277 K is given for comparison in Fig. 2 additionally. It exhibits a maximum at 3.4 Å and a pronounced shoulder at approximately 3.7 Å. The ex-

Table 2. Characteristic values of the radial distribution functions $g_{\alpha\beta}(r)$ for the Li^+-ammonia solution. R_i, r_{M_i} and r_{m_i} are the distances in Å, where for the ith time $g_{\alpha\beta}(r)$ is unity, has a maximum and minimum, respectively. The values for g_{LiO} and g_{LiH} are taken from the simulation of a 2.2 molal aqueous LiI solution [21] and are included for comparison.

$\alpha\beta$	T/K	R_1	r_{M_1}	$g_{\alpha\beta}(r_{M_1})$	R_2	r_{m_1}	$g_{\alpha\beta}(r_{m_1})$	r_{M_2}	$g_{\alpha\beta}(r_{M_2})$	$n_{\alpha\beta}(r_{m_1})$
NN	235	3.04	3.38	2.2	4.29	5.0	0.72	6.64	1.17	12.8
	277	3.04	3.36	1.9	4.35	5.0	0.78	6.64	1.20	12.0
NH	235	3.11	3.62	1.3	4.47	4.9–5.3	0.8	–	–	34.2–43.4
	277	3.04	3.69	1.3	4.58	4.9–5.4	0.9	–	–	32.4–42.3
HH	235	3.07	3.82	1.2	4.56	5.0–5.5	0.9	–	–	36.5–47.6
	277	3.22	3.87	1.2	4.69	5.2–5.4	0.9	–	–	37.0–42.0
LiN	235	2.01	2.29	15.9	2.53	2.8	0.0	4.38	2.99	6.0
	277	2.02	2.20	13.6	2.53	2.9	0.0	4.64	2.34	6.0
LiH	235	2.54	2.87	6.5	3.16	3.4	0.04	5.0	1.97	18.0
	277	2.54	2.80	6.9	3.17	3.6	0.07	5.02	1.64	18.1
LiO	305	1.98	2.12	16.9	2.38	2.9	0.0	4.91	2.04	6.1
LiH	305	2.46	2.68	7.4	2.97	3.2	0.55	4.82	1.46	13.1

perimental coordination number of 12 is indicative of a close-packed nearest neighbour arrangement. The MD results at 277 K agree well with the X-ray data as far as position and height of the first maximum and the coordination number is concerned, which is taken as the value of the running integration number at the position of the first minimum of the RDF (see Table 2). However, the simulated RDF shows substantial contributions around 3 Å which are absent in Narten's experimental data. This disagreement might result from an insufficient hardness of the pair potential. Due to the absence of reliable neutron scattering data the usefulness of the potentials describing the N–H and H–H interactions cannot be checked. Therefore, it does not seem appropriate at present to try to improve the potentials in a way as to achieve better agreement with the X-ray data only.

The N–N nearest neighbor distances resulting from two of the other simulations [6, 9] agree in the limits of uncertainty with the ones found in this work and the X-ray measurement, while those reported in [7] and [8] are smaller by about 0.2 Å. All coordination numbers calculated range from 12 to 13.

The $g_{NH}(r)$ and $g_{HH}(r)$ show only a small deviation from a uniform distribution and consequently the simulated RDFs for the two temperatures differ significantly only in $g_{NN}(r)$ (Figure 2). The increase in the height of the first maximum indicates a slightly more pronounced first neighbor structure at the lower temperature. The shoulder in $g_{NH}(r)$ at approximately 2.3 Å corresponds to the first maximum of the oxygen-hydrogen RDF in water [18]. The fact that, contrary to the water case, the first and second peak in $g_{NH}(r)$ are not separated and the shoulder is only weakly pronounced, shows the relatively low contribution of hydrogen bonding to the structure of ammonia. This is in agreement with the value of 12 for the coordination number which also favours the picture of a close-packed structure rather than an open hydrogen bond network. The higher coordination number at the lower temperature can be accounted for by the about 9% higher density at 235 K.

In order to investigate in more detail the solvent structure around a central NH_3 molecule the nitrogen-nitrogen and nitrogen-hydrogen RDFs are shown in Fig. 3 for the two half-spaces which are separated by a plane which contains the central N atom and which is perpendicular to the dipole vector of the central molecule. The positions of the maxima in $g_{NN}(r)$ for the two subsystems are only slightly different but the distribution of N–N distances on the lone pair side is broader than on the hydrogen atom side just as expected from water [19]. This difference in width is responsible for the shoulder in the total $g_{NN}(r)$. The running integration number for both half-spaces is practically identical for all distances r in agreement with a close-packed structure. Naturally, the two $g_{NH}(r)$ are significantly different. The hump in $g_{NH}(r)$ around 2.3 Å is obviously due to those hydrogens which are located on the lone-pair side of the central molecule. Consequently there is a phase shift in the positions of the maxima and minima which leads to an interference effect resulting in a strong tendency towards a uniform distribution in the total $g_{NH}(r)$ (Figure 2). The running coordination numbers for the two subsystems are approximately the same at a distance of about 5 Å.

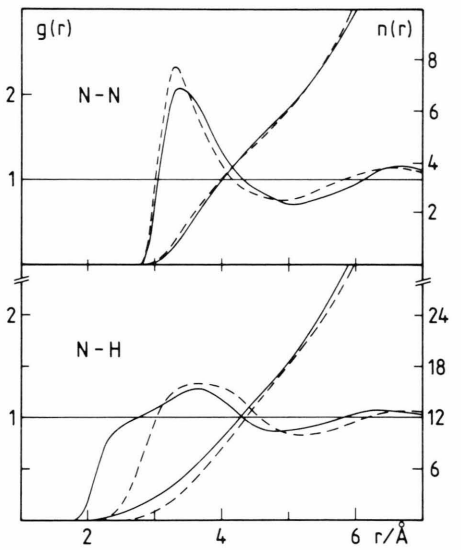

Fig. 3. Nitrogen-nitrogen and nitrogen-hydrogen radial distribution functions and running integration numbers for a Li^+-ammonia solution at 235 K, computed for pairs where the second atom is on the lone pair side (full) and on the proton side (dashed). For further details see text.

In order to calculate from the simulation the time averaged geometrical arrangement of the nearest neighbor NH_3 molecules around a central one, a molecule based coordinate system has been introduced in such a way that the negative z-axis coincides with the dipole moment direction and one hydrogen atom defines the y-axis (insertion in Figure 4). The polar coordinates (r, ϑ, φ) of the nitrogen atoms of the neighboring NH_3 molecules are calculated in this coordinate

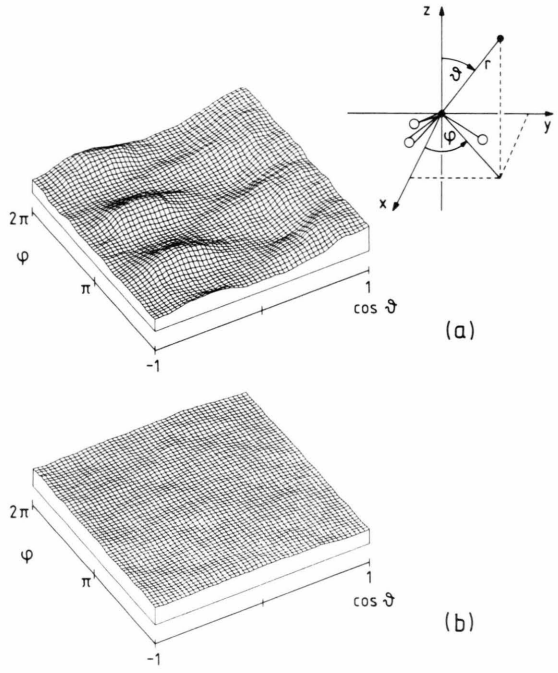

Fig. 4. Probability densities in $\cos\vartheta$ and φ for the positions of the nitrogen atoms around a central NH_3 molecule for two different ranges of N–N distances (a: $r \leq 3.5$ Å; b: 4.0 Å $\leq r \leq$ 5.0 Å). The definition of the molecule fixed coordinate system is shown in the insertion.

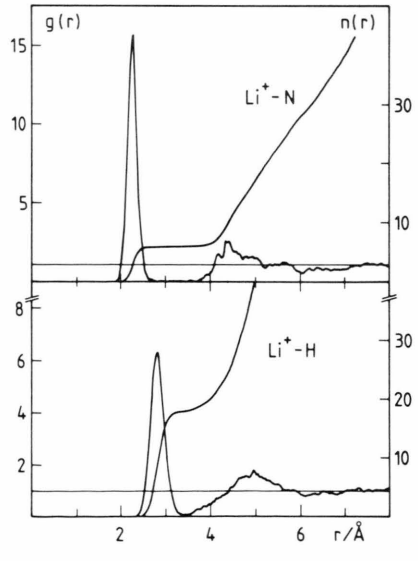

Fig. 5. Ion-nitrogen and ion-hydrogen radial distribution functions and running integration numbers for a Li^+-ammonia solution at 235 K.

system at several hundred time steps spread over the whole simulation run and their probability densities in $\cos\vartheta$ and φ are shown in Fig. 4 for two different ranges of N–N distances (a: $r \leq 3.5$ Å; b: 4 Å $\leq r \leq$ 5 Å). The procedure is similar to the one used by Pálinkás and Heinzinger in case of water (see e.g. [19, 20]). The probability densities in Fig. 4a show a set of 3 maxima at φ-values of about 90°, 210°, and 330° in the ϑ-range 110°–125°. These locations can be easily identified with the N–H directions and indicate a small preference for linear hydrogen bonds. The nearest neighbor nitrogen atoms on the lone pair side ($\cos\vartheta > 0$) do not seem to have a significant preference as far as φ is concerned. Figure 4b demonstrates that the nitrogen atoms beyond 4 Å are uniformly distributed around the central NH_3 molecule. Again, it can be concluded that the structure of ammonia can best be described as that of a close packed liquid with small disturbances due to hydrogen bonding between closest neighbours.

b) Solvation Shell Structure of the Lithium Ion

In Fig. 5 the Li–N and Li–H RDFs and the corresponding running integration numbers for 235 K are depicted. A well pronounced first solvation shell with a Li–N distance of 2.29 Å exists as can be seen from the narrow and high first maximum. The first peak in $g_{LiN}(r)$ is slightly lower than that of $g_{LiO}(r)$ in water at 305 K [21] (Table 2). The existence of a second solvation shell is indicated. Integration of $g_{LiN}(r)$ and $g_{LiH}(r)$ over the first solvation shell yields 6 and 18 neighbours, respectively. The coordination number of six points to an octahedral arrangement of solvent molecules similar to the one found for the hydration shell of Li^+ [20]. Recently, Impey et al. [11] calculated a coordination number of 4 from an MD simulation of a solution of one lithium ion in 107 NH_3 molecules. This simulation was performed, however, using an empirical ion-NH_3 potential where the corresponding parameters were transferred from the ion-water potential.

Only slight differences in the $Li^+ - NH_3$ RDFs have been found between the two temperatures, therefore the RDFs for 277 K are not depicted in Figure 5. The coordination number at 277 K is the same as that at 235 K (Table 2).

Figure 6 shows the distribution of $\cos\theta$ for the NH_3 molecules in the first solvation shell of Li^+. θ is defined as the angle between the dipole moment direction of

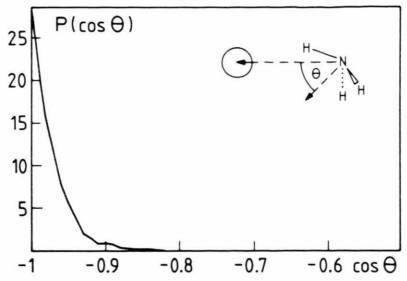

Fig. 6. Distribution of $\cos\theta$ for the ammonia molecules in the first solvation shell of Li^+. θ is defined in the insertion, the circle is Li^+.

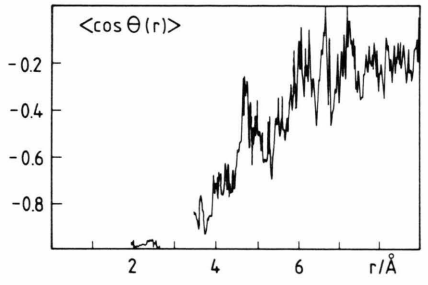

Fig. 7. Average values of $\cos\theta$ as a function of the ion-nitrogen distance. θ is defined in Figure 6.

the ammonia molecule and the vector pointing from the nitrogen atom towards the center of the ion. The distribution has a sharp maximum at $\cos\theta = -1$ which indicates a dipole ordered solvation shell. Similar results were reported recently by Impey et al. [11]. A dipole ordered hydration shell has also been found in simulations of highly concentrated aqueous LiCl solutions [22, 23].

The range of preferential orientation of NH_3 around Li^+ can be seen from Fig. 7, where the average value of $\cos\theta$ is plotted as a function of the Li–N distance. $\cos\theta$ is about -1 over the range of the first solvation shell, as expected from Fig. 6, and decays slowly beyond 4 Å towards a limiting value of -0.2. The preferential orientation extends to longer distances here than e.g. in a 2.2 molal aqueous LiI solution [21]. This difference could be caused either by the higher ionic concentration in the LiI solution or the weaker solvent-solvent interactions in the case of ammonia.

c) Intramolecular Geometry

The flexible model for the ammonia molecule permits the investigation of the effect of the cation on the

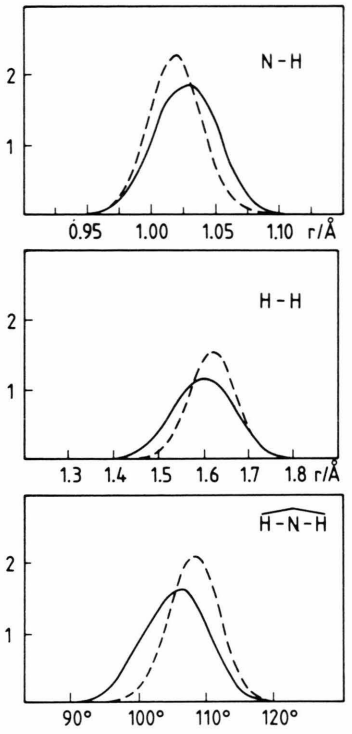

Fig. 8. Normalized distributions of the intramolecular N–H (top) and H–H (center) distances and HNH angles (bottom) in arbitrary units, calculated separately for ammonia molecules in the bulk (dashed) and in the solvation shell of Li^+ (full).

molecular geometry. In Fig. 8 the distributions of the N–H distances (top), H–H distances (center) and HNH angles (bottom) are depicted, calculated separately for molecules in the first solvation shell of Li^+ (full) and in the bulk (dashed). In the solvation shell the average N–H bond length is increased from 1.01 Å to 1.02 Å and the H–H distance and the HNH angle are decreased. These changes in geometry result in an average value of the dipole moment in the solvation shell of Li^+ of 1.85 D compared with a bulk value of 1.60 D and a gas phase value of 1.47 D. Similar differences in the dipole moments between gas phase, bulk and hydration shells of ions have been found from simulations of water and aqueous electrolyte solutions [22].

d) Translational Motion

The dynamical properties of the solution are conveniently calculated from the simulation through time

correlation functions. For a system of N particles the time dependent autocorrelation function (acf) of a property A is calculated by

$$c_A(t) = < A(0) \cdot A(t) > = \frac{1}{N \cdot N_T} \sum_{i=1}^{N_T} \sum_{j=1}^{N} A_j(t_i) \cdot A_j(t_i + t), \quad (4)$$

where N_T is the number of time origins t_i.

In Fig. 9 the normalized center-of-mass velocity acfs of the ammonia molecules are presented separately for the bulk phase and for the solvation shell of the Li^+. The differences are much stronger than in the case of aqueous electrolyte solutions [24]. For bulk ammonia (top) $c_v(t)$ decays to zero over a time range of about 0.2 ps and remains zero except for statistical noise. This behavior indicates a relatively free translational motion and is in agreement with the conclusion drawn above that hydrogen bonding effects are not very important for the structure of the solution. The strong interactions of the ammonia molecules with the lithium ion in the solvation shell lead to pronounced oscillations in the acf (bottom).

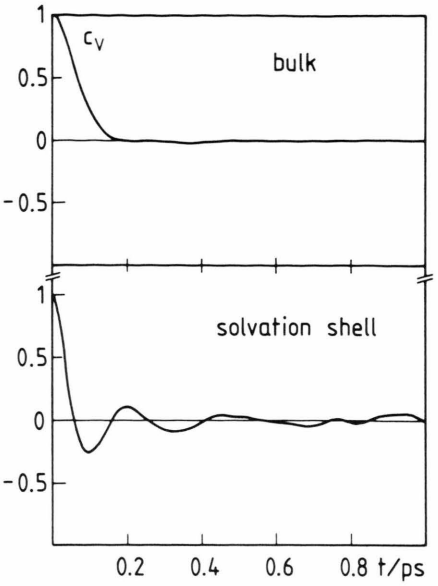

Fig. 9. Normalized center-of-mass velocity autocorrelation functions, calculated separately for bulk ammonia and ammonia in the solvation shell of Li^+.

The spectral densities of the hindered translational motions have been calculated by Fourier transformation of the velocity acfs according to

$$f(\omega) = \int_0^\infty c_v(t) \cos(\omega t)\, dt. \quad (5)$$

They are shown in Fig. 10, again separately for the bulk and the solvation shell. In bulk ammonia the maximum at zero frequency is expected from the corresponding acf in Fig. 9 and is a consequence of the weak interaction between ammonia molecules. In the solvation shell a maximum of the spectral density at about 140 cm^{-1} is observed. This value lies within the range of the broad band found for water in the hydration shell of Li^+ (about 50 to 250 cm^{-1}) [24].

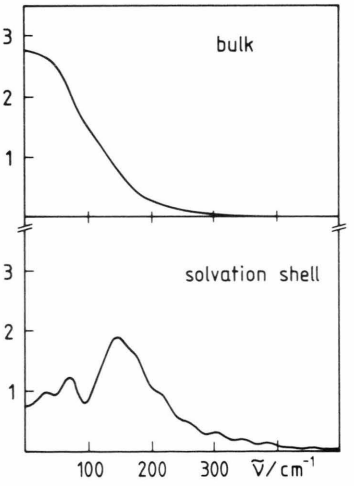

Fig. 10. Spectral densities of hindered translational motions in arbitrary units, calculated separately for bulk ammonia and ammonia in the solvation shell of Li^+.

The self-diffusion coefficient D can be calculated from the Green-Kubo relation

$$D = \frac{1}{3} \lim_{t \to \infty} \int_0^t c_v(t')\, dt', \quad (6)$$

where c_v is the center-of-mass velocity acf. Beyond about $t = 1.5$ ps $c_v(t)$ is zero except for statistical noise. The D values calculated from the present simulation for 235 K are $(9.0 \pm 0.3) \cdot 10^{-5}$ $cm^2\,s^{-1}$ and $(1.9 \pm 0.5) \cdot 10^{-5}$ $cm^2\,s^{-1}$ for bulk and solvation shell ammonia, respectively. The relatively large error for the solvation shell is due to the fact that there are only six ammonia molecules contributing to the statistics. The large discrepancy between the bulk phase value and the experimental one for pure liquid ammonia of $D = 5.3 \cdot 10^{-5}$ $cm^2\,s^{-1}$ [25] is at present not fully understood. One reason might be that the ammonia-ammonia potential employed in this simulation is not sufficiently negative.

e) Librational Motions

The spectral densities of librational and vibrational motions can be calculated from a simulation with flexible molecules by Fourier transformation of the velocity autocorrelation functions of the hydrogen atoms.

As this method does not allow for an unambiguous separation of the different rotational modes (e.g. rotations around the three molecule fixed axes as defined in the insertion of Fig. 4) a scheme has been used, originally developed by Bopp for CF water [26, 27], where after subtraction of the center-of-mass velocity of the molecule the velocities of the hydrogen atoms are projected onto the molecule-fixed axes. Details are given in Appendix B.

The spectral densities of the librational motions of ammonia in the bulk and in the solvation shell are presented in Fig. 11 for the rotation about the two degenerate axes x and y (top) and that about the dipole moment axis z (bottom). For the rotation about the degenerate axes a strong cation effect is found. The frequency increases from about $180\,cm^{-1}$ in the bulk to about $390\,cm^{-1}$ in the solvation shell of the Li^+. The rotation about the dipole axis (bottom) remains practically unchanged. The maximum at zero frequency indicates a rather free rotational motion.

These differences between bulk and solvation shell of Li^+ for the two modes can be understood easily on the basis of the structure of the solution as discussed above. Strong solvation forces keep the dipole vector antiparallel to the $N-Li^+$ vector, with θ very close to 180° (Figure 6). Thus, the Li^+-ammonia interactions hinder the motion around the x- and y-axis, but do not influence the rotation around the dipole axis.

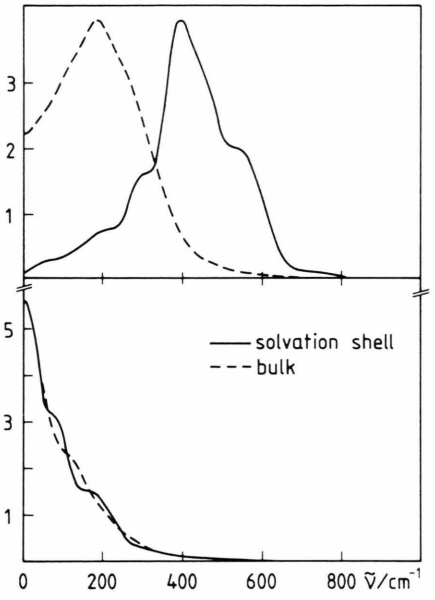

Fig. 11. Spectral densities of the librational motions about the x- or y-axis (top) and the z-axis (bottom) of ammonia molecules in arbitrary units, calculated separately for bulk ammonia (dashed) and ammonia in the solvation shell of Li^+ (solid). The molecule fixed coordinate system is defined in the insertion of Figure 4.

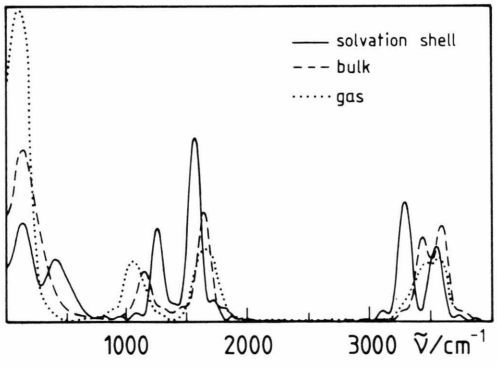

Fig. 12. Fourier transforms of the hydrogen velocity autocorrelation functions for bulk ammonia (dashed), ammonia in the Li^+ solvation shell (full) and ammonia in the gas phase (dotted) from a simulation at 235 K.

f) Intramolecular Vibrations

The total spectral densities calculated from the hydrogen atom acfs of NH_3 in the bulk, in the solvation shell, and in the gas phase (simulation without intermolecular interactions) are shown in Figure 12. Besides the intermolecular frequency range (translations and rotations, below $700\,cm^{-1}$), which has been discussed above, a HNH bending region (from 700 to $2000\,cm^{-1}$) and a N–H stretching region (from 3000 to $4000\,cm^{-1}$) can be distinguished. From a symmetry coordinate analysis which will be reported in a different communication [28] and which is similar to that developed by Bopp [26] for water the symmetric and the asymmetric stretching and bending modes can be unambiguously identified. The frequencies calculated from the simulation are presented in Table 3.

The effect of a single ion on the intramolecular vibrations of its solvation shell molecules cannot be measured directly, its investigation is one of the advantages of MD simulations. The reliability of the ion induced frequency shifts calculated from the simulation is largely determined by the potentials employed

Mode	MD($Li^+ - NH_3$)			expt. (pure NH_3)	
	solvation shell	bulk liquid	gas	liquid [29]	gas [14]
sym. bend	1260	1125	1040	1066	932, 968
asym. bend	1565	1630	1640	1638	1627
sym. stretch	3300	3400	3440	3240	3336
asym. stretch	3550	3565	3570	3379	3444

Table 3. Comparison of various vibrational frequencies calculated from the simulation separately for ammonia molecules in the first solvation shell of Li^+, the bulk liquid, and in the gas phase with experimental results.

in the simulations. Their quality can only be checked by comparison with experimental results as far as they can be deduced unambiguously from measurements.

Therefore, the various vibrational frequencies calculated from the simulation for NH_3 in the bulk and in the gas phase are compared in Table 3 with IR data [14, 29]. For this comparison it is important to know that the statistical uncertainties in the calculated frequencies are estimated to be about $\pm 20\,cm^{-1}$. With this error margin the following statements can be made: In simulation and experiment all symmetric modes are found at lower frequencies than the corresponding asymmetric ones, as expected. The differences between symmetric and asymmetric modes are in the case of the simulated frequencies about $75\,cm^{-1}$ smaller for the bends and about $25\,cm^{-1}$ larger for the stretches when compared with the experimental results for both gas phase and liquid. The measured and simulated gas-liquid frequency shifts are practically zero for the asymmetric bend and show qualitative agreement as far as a blueshift of the symmetric bend and a redshift of the symmetric stretch are concerned. The redshift of $65\,cm^{-1}$ of the asymmetric stretch was not reproduced by the simulation.

From this qualitative agreement between simulated and measured frequencies it can be expected that the potentials employed in the simulation lead to a qualitatively correct description of the effect of Li^+ on the intramolecular properties of the NH_3 molecules in its first solvation shell. As can be read from Table 3, the frequency of the asymmetric stretching mode remains uneffected by Li^+. The asymmetric bending and the symmetric stretching modes are redshifted in the solvation shell by 65 and $100\,cm^{-1}$, respectively, while the symmetric bend shows a blueshift of $135\,cm^{-1}$. The redshift of the stretching frequency is in agreement with the increase of the average N–H distance in the solvation shell by 0.01 Å (Fig. 8). The interactions between Li^+ and the flexible NH_3 molecules in its first solvation shell result in an attractive force on the N atom and repulsive ones on the H atoms. Different from the bulk, there exists additionally a repulsion between the H atoms of the strongly oriented NH_3 molecules in the first solvation shell (Figure 6). Both effects lead to a smaller average HNH angle relative to the bulk molecules (Figure 8). In the symmetric bending motion all HNH angles increase or decrease simultaneously. The repulsion between the hydrogen atoms should thus be more important in the symmetric bend than in the asymmetric bends (where the effects partly cancel as always two angles increase and one decreases or vice versa). Consequently, the symmetric bending motion is shifted more to the blue than the asymmetric one in the solvation shell. The actually occuring redshift of the asymmetric bending mode is, however, not fully understood at the moment. The weak interaction between ammonia molecules is demonstrated here again by the fact that all frequency shifts between bulk and solvation shell of Li^+ are larger than the gas-liquid ones.

A similar detailed analysis of the effect of ions on the intramolecular vibrations of the molecules in their first solvation shells has been reported up to now only for an aqueous $CaCl_2$ solution [26]. For the water molecules in the hydration shell of Ca^{2+} a redshift relative to bulk water of about $300\,cm^{-1}$ has been found not only for the symmetric but also for the asymmetric stretching mode. This is in accordance with the lengthening of the O–H distance by 0.02 Å. It is the Cl^- which induces a similar effect on water as the Li^+ on the first shell NH_3 molecules, namely a $75\,cm^{-1}$ redshift for the symmetric and no shift for the asymmetric stretch. The bending mode of water is hardly affected by the ions, again significantly different from the results reported here. There seems to be no easy explanation for the differences between the effect of Li^+ on NH_3 and Ca^{2+} as well as Cl^- on water.

Finally, it can be inferred from the absence of any HNH angles of 120° or more in the HNH angle distribution function (Fig. 8) that during the simulation time of 3.75 ps no inversion of ammonia molecules has occured. This result is expected on the basis of the fact that the period of inversion is about 21 ps [30].

Acknowledgements

SVH and TI thank the Max-Planck-Gesellschaft and SVH additionally the Chulalongkorn University for fellowships. ES gratefully acknowledges financial support by Deutsche Forschungsgemeinschaft and TI by the U.S. Department of Energy, Office of Basic Energy Sciences (DE-AC02-80ER10612). We would like to thank Dr. P. Bopp for helpful discussions.

Appendix A

All non-zero force constants of the intramolecular force field of ammonia occurring in (1) are summarized here. They have been calculated from the parameters given in [14]. The values are such that the forces are in units of mdyn when the displacements Δr_i are in Å and the angle changes $\Delta\alpha_i$ are in radian.

Inversion force constants

$k_1 = -0.53741$
$k_2 = +2.08241$
$k_3 = -0.77902$
$k_4 = +0.35000$
$k'_1 = +1.0806$
$k'_2 = -5.7569$

Second-order force constants

$F_{11} = 6.8186$
$F_{22} = F_{44} = 6.8975$
$F_{33} = F_{55} = 0.6166$
$F_{23} = F_{45} = 0.0028$

Third-order force constants

$F_{111} = -3.92836$
$F_{122} = F_{144} = -11.9988$
$F_{123} = F_{145} = -4.8718 \cdot 10^{-3}$
$F_{133} = F_{155} = -0.10989$
$F_{222} = -2.82914$
$F_{244} = 8.4874$
$F_{223} = -F_{344} = 5.9505 \cdot 10^{-6}$
$F_{245} = 1.1901 \cdot 10^{-5}$
$F_{233} = -F_{255} = -1.0983 \cdot 10^{-3}$
$F_{345} = 2.1966 \cdot 10^{-3}$
$F_{333} = -0.06747$
$F_{355} = 0.2024$

Fourth-order force constants

$F_{1111} = 2.8351$
$F_{1122} = F_{1144} = 17.163$
$F_{1133} = F_{1155} = 0.08564$
$F_{1222} = 8.1277$
$F_{1244} = -24.3830$
$F_{1333} = 0.01625$
$F_{1355} = -0.04875$
$F_{2222} = F_{4444} = 4.3066$
$F_{2244} = 8.6133$
$F_{2233} = F_{2255} =$
$F_{3344} = F_{4455} = 0.04078$
$F_{3333} = F_{5555} = 0.08044$
$F_{3355} = 0.16087$

Appendix B

In order to calculate the angular velocities about the three principal axes of an ammonia molecule the following scheme has been used: Let Z_i denote the projections of the hydrogen velocities on the dipole axis $\hat{\mu}$,

$$Z_i = (\vec{v}_{H_i} \cdot \hat{\mu}), \quad i = 1, 3 \tag{B1}$$

and P_i denote the projection of the hydrogen velocity on a vector $\hat{e}_i$ which is perpendicular to a plane spanned by the center of mass, the nitrogen and hydrogen i,

$$P_i = (\vec{v}_{H_i} \cdot \hat{e}_i), \ \hat{e}_i = (\hat{\mu} \times \hat{r}_{NH_i}), \ i = 1, 3. \tag{B2}$$

where $\hat{r}_{NH_i}$ is the $N-H_i$ distance vector.

Certain symmetry-adapted linear combinations of these velocity components are approximately proportional (if one assumes that the distortions of molecules in the liquid are not too large) to the orbital velocities of rotation about the 3 molecule-fixed principal axes:

$$\begin{aligned} R_x &= \frac{1}{\sqrt{6}}(2Z_1 - Z_2 - Z_3), \\ R_y &= \frac{1}{\sqrt{2}}(Z_2 - Z_3), \\ R_z &= \frac{1}{\sqrt{3}}(P_1 + P_2 + P_3), \end{aligned} \tag{B3}$$

where the molecular yz-plane is defined by the center of mass, the nitrogen, and hydrogen atom 1. By symmetry, R_x and R_y are degenerate.

[1] J. C. Thompson, Electrons in Liquid Ammonia, Clarendon Press, Oxford 1976.
[2] J. A. Morgan, R. L. Schroeder, and J. C. Thomson, J. Chem. Phys. **43,** 4494 (1965).
[3] A. H. Narten, J. Chem. Phys. **66,** 3117 (1977).
[4] P. Chieux and H. Bertagnolli, J. Phys. Chem. **88**, 3726 (1984).
[5] F. H. Stillinger, Israel J. Chem. **14,** 130 (1975).
[6] M. L. Klein and I. R. McDonald, J. Chem. Phys. **74,** 4214 (1981).
[7] (a) A. Hinchliffe, D. G. Bounds, M. L. Klein, I. R. McDonald, and R. Righini, J. Chem. Phys. **74,** 1211 (1981); (b) R. W. Impey and M. L. Klein, Chem. Phys. Lett. **104,** 579 (1984); (c) M. L. Klein, I. R. McDonald, and R. Righini, J. Chem. Phys. **71,** 3673 (1979).
[8] W. L. Jorgensen and M. Ibrahim, J. Amer. Chem. Soc. **102,** 3309 (1980).
[9] K. P. Sagarik, P. Ahlrichs, and S. Brode, Mol. Phys. **57,** 1247 (1986).

[10] M. Sprik, R. W. Impey, and M. L. Klein, J. Chem. Phys. **83,** 5802 (1985).
[11] R. W. Impey, M. Sprik, and M. L. Klein, J. Amer. Chem. Soc. **109,** 5900 (1987).
[12] W. S. Benedict and E. K. Plyler, Can. J. Phys. **35,** 890 (1985).
[13] P. Bopp, D. R. McLaughlin, and M. Wolfsberg, Z. Naturforsch. **37a,** 398 (1982).
[14] V. Spirko, J. Mol. Spectrosc. **101,** 30 (1983).
[15] B. Maessen, P. Bopp, D. R. McLaughlin, and M. Wolfsberg, Z. Naturforsch. **39a,** 1005 (1984).
[16] S. V. Hannongbua, S. U. Kokpol, S. Kheawsrikul, S. Polman, and B. M. Rode, Z. Naturforsch. **43a,** 143 (1988).
[17] W. B. Streett, D. J. Tildesley, and G. Saville, ACS Symp. Ser. **86,** 144 (1978).
[18] F. H. Stillinger and A. Rahman, J. Chem. Phys. **60,** 1545 (1974).
[19] K. Heinzinger and G. Pálinkás, in: Interactions of Water in Ionic and Nonionic Hydrates (H. Kleeberg, ed.), Springer-Verlag, Berlin 1987, 1–22.
[20] Gy.I. Szász, K. Heinzinger, and G. Pálinkás, Chem. Phys. Lett. **78,** 194 (1981).
[21] Gy.I. Szász, K. Heinzinger, and W. O. Riede, Z. Naturforsch. **36a,** 1067 (1981).
[22] P. Bopp, I. Okada, H. Ohtaki, and K. Heinzinger, Z. Naturforsch. **40a,** 116 (1985).
[23] K. Tanaka, N. Ogita, Y. Tamura, I. Okada, H. Ohtaki, G. Pálinkás, E. Spohr, and K. Heinzinger, Z. Naturforsch. **42a,** 29 (1987).
[24] Gy.I. Szász and K. Heinzinger, J. Chem. Phys. **79,** 3467 (1983).
[25] A. N. Garroway and R. M. Cotts, Phys. Rev. **A7,** 635 (1973).
[26] P. Bopp, Chem. Phys. **196,** 205 (1986).
[27] P. Bopp, Habilitationsschrift, Technische Hochschule Darmstadt, Darmstadt 1987.
[28] P. Bopp and E. Spohr, to be published.
[29] T. Birchall, I. Drummond, J. Chem. Soc. **A1970,** 1859.
[30] J. M. Hollas, High Resolution Spectroscopy, Butterworth, London 1982.